npj | parkinson's disease

Article

Published in partnership with the Parkinson's Foundation

https://doi.org/10.1038/s41531-025-01058-0

Cortical macro- and microstructural changes in isolated rapid eye movement sleep behavior disorder

Jèssica Pardo[1,2,13], Ignacio Roura[1,2,13], Victor Montal[3,4], Cristina Martín-Barceló[1,2], Javier Oltra[1,2,5], Anna Campabadal[1,2,6], Núria Bargalló[2,7,8], Mònica Serradell[9], Gerard Mayà[9], Angelica Montini[9], Carles Gaig[2,9], Claustre Pont-Sunyer[10], Juan Fortea[3,11,12], Alex Iranzo[2,9,11] ✉, Carme Junqué[1,2,11] & Bàrbara Segura[1,2,11] ✉

Cortical mean diffusivity (cMD), a marker of cortical microstructural changes in neurodegenerative disorders, remains unexplored in isolated REM sleep behavior disorder (iRBD), a prodromal stage of Lewy body (LB) diseases. Its relationship with cortical thickness (CTh), clinical features, and neuropsychological performance is also unknown. We assessed cMD and CTh in thirty-six patients with iRBD at high risk of conversion and 29 healthy controls (HC), examining associations with clinical and cognitive measures. Effect sizes were calculated using Cohen's *d*. Patients with iRBD showed increased cMD in rostral and caudal cortical regions compared to HC ($d > 0.5$). Cortical thinning was restricted to caudal areas. Higher cMD correlated with longer iRBD duration, later onset, MDS-UPDRS III, apathy, and poorer performance on Grooved Pegboard and Symbol-Digit Modality Tests. These findings suggest that cMD may be more sensitive than CTh and serve as a valuable imaging biomarker for detecting early cortical changes in prodromal LB diseases.

Isolated rapid eye movement (REM) sleep behavior disorder (iRBD) is a parasomnia characterized by a dysfunction of the neurophysiology underlying REM sleep that results in enacting dreams and vigorous motor activity due to the loss of muscle atonia[1,2]. This condition is a widely recognized prodromal stage of alpha-synucleinopathies[3–5]. The risk of conversion has been estimated to be over 90% in studies with long-term follow-up[6], with conversion rates around 44–57% to Parkinson's disease (PD), 25–45% to dementia with Lewy bodies (DLB), and 5–6% to multiple system atrophy (MSA)[6–12].

Understanding the prodromal phases of neurodegenerative diseases[3,13] and identifying progression markers is crucial for clinical practice, clinical trials, patient selection, and surrogate markers of efficacy[14–16]. iRBD is a prodromal condition of overt alpha-synucleinopathies[17] that offers unique opportunities for identifying prognostic biomarkers for Lewy body (LB) diseases[18]. The interest is especially focused on identifying patients at higher risk of phenoconversion, considering the long latency of this condition[19]. The Movement Disorders Society (MDS) has developed a validated algorithm to predict phenoconversion[16,20], with a sensitivity of 81.3% and a specificity of 67.9% for PD or DLB at a 4-year follow-up[16]. Cognition and neuroimaging have been proposed as interesting biomarkers due to their sensitivity, specificity, reproducibility, cost-effectiveness, and availability[18].

Different approaches have used structural MRI in iRBD to predict phenoconversion to LB disorders. Degeneration of brain regions beyond the brainstem nuclei is expected as this disorder progresses, affecting the

[1]Medical Psychology Unit, Department of Medicine, Institute of Neurosciences, University of Barcelona, Barcelona, Spain. [2]Fundació de Recerca Clínic Barcelona-Institut d'Investigacions Biomèdiques August Pi i Sunyer (FRCB-IDIBAPS), Barcelona, Spain. [3]Sant Pau Memory Unit, Department of Neurology, Hospital de la Santa Creu i Sant Pau, Biomedical Research Institute Sant Pau, Universitat Autònoma de Barcelona, Barcelona, Spain. [4]Department of Life Sciences, Barcelona Supercomputing Center, Barcelona, Spain. [5]Aging Research Center, Department of Neurobiology, Care Sciences, and Society, Karolinska Institutet and Stockholm University, Stockholm, Sweden. [6]Neurology Service, Consorci Corporació Sanitària Parc Taulí de Sabadell, Barcelona, Spain. [7]Imaging Diagnostic Center (CDI), Hospital Clínic Universitari de Barcelona, Barcelona, Spain. [8]Centro de Investigación Biomédica en Red de Salud Mental (CIBERSAM), Instituto de Salud Carlos III, Madrid, Spain. [9]Sleep Disorders Center, Neurology Service, Hospital Clínic Universitari de Barcelona, University of Barcelona, Barcelona, Spain. [10]Servei de Neurologia Unitat de Trastorns del Moviment, Fundació Privada Hospital Asil de Granollers, Barcelona, Spain. [11]Centro de Investigación Biomédica en Red sobre Enfermedades Neurodegenerativas, Barcelona, Spain. [12]Barcelona Down Medical Center, Fundació Catalana de Síndrome de Down, Barcelona, Spain. [13]These authors contributed equally: Jèssica Pardo, Ignacio Roura.
✉e-mail: airanzo@clinic.cat; bsegura@ub.edu

striatum, substantia nigra (SN), limbic system, and cortex, which suggests a widespread neurodegenerative process[21,22]. The current gold-standard techniques to study cortical neurodegeneration are cortical thickness (CTh) measurements and voxel-based morphometry (VBM), which have shown rostral and caudal neurodegeneration in iRBD[23], involving the frontal[24–27], occipital[24,27–30], temporal[24,27,28], parietal[28,29,31], and cingulate[24,25] cortices.

Furthermore, longer iRBD duration and younger age at onset have been associated with gray matter atrophy in rostral regions[23,25]. In contrast, older age at onset has been related to cortical thinning in caudal regions[31]. Concerning neuropsychological performance, several studies have found associations between cortical thinning and impaired attention and executive functions[26], verbal learning[26,29], visuospatial abilities[26,29,31], motor skills[25], and hyposmia[29] in patients with iRBD compared to HC. Although CTh has been considered sensitive to detecting cortico-structural brain changes[23] and distinguishing between clinical iRBD subtypes[18], findings to date are insufficient to identify consistent patterns of degeneration across studies. This could be due to the difficulty in detecting cortical atrophy at the individual level at diagnosis, the different disease stages among patients, and the high inter-individual variability in cortical atrophy patterns in alpha-synucleinopathies[32]. Since diffusion-weighted imaging (DWI) detects microscopic changes, and microstructural alterations suggest early cognitive decline more than macrostructural atrophy, DWI techniques could offer supplementary insights to the commonly used macrostructural techniques[33]. This is especially relevant in the investigation of prodromal stages of neurodegenerative diseases.

Cortical mean diffusivity (cMD) is a useful surface-based diffusion approach previously used to study the cortical microstructure of the brain in different neurodegenerative diseases[33–44]. Neurodegenerative diseases involve microstructural disorganization, cellular death, demyelination, and neuronal damage, inevitably leading to the collapse of water diffusion brain barriers[33–36,43,45]. We have previously shown that cMD is capable of detecting cortical abnormalities better than CTh approaches in several neurodegenerative diseases, focusing on specific regions[41] or the entire brain[33,35,44]. Recently, this technique has been used in PD[45–48] with and without RBD[49]. Furthermore, several studies on Alzheimer's disease (AD) have pioneered the investigation of its prodromal stages using cMD[34,37,41,50].

Nevertheless, cMD has not yet been tested in patients with iRBD. We hypothesize that cMD would better characterize structural cortical changes than CTh and would be associated with clinical manifestations and cognitive outcomes of patients with iRBD at a high risk of conversion to alpha-synucleinopathies.

The main purpose of this study was to (1) characterize cortical microstructural and macrostructural changes in patients with iRBD at a high risk of conversion to LB diseases, and (2) establish a relationship with their clinical features and neuropsychological performance.

Results

Sample composition and demographics

The final sample was composed of 36 patients with iRBD at high risk of conversion to LB pathology and 29 age- and sex-matched HC. Eight patients with iRBD were excluded due to MMSE score below 25 ($n = 4$), MRI movement ($n = 1$), and missing data ($n = 3$).

Table 1 summarizes the sociodemographic and clinical characteristics of the participants. There were no statistically significant differences between groups in age, sex, years of education, or premorbid intelligence. Patients with iRBD showed lower scores in global cognition, higher scores for non-motor symptoms, depression, apathy, and neuropsychiatric comorbidities, and poorer performance in olfactory function.

Neuropsychological performance

Table 2 describes neuropsychological differences between groups. Patients with iRBD showed poorer performance than HC in the Digits forward span subtest of the Wechsler's Adult Intelligence Scale-IV (WAIS-IV), Similarities subtest (WAIS-IV), Symbol Digit Modalities Test (SDMT), Stroop Word and Color subtests, semantic fluency (animals), Rey's Auditory Verbal Learning Test (RAVLT) false recognition, Clock copying test, dominant and non-dominant Grooved Pegboard test (GPT), and Reading the Mind in the Eyes Test (RMET). Patients with iRBD also showed worse performance in the Boston Naming Test (BNT), phonetic fluency (letter "P"), and the total score of the RAVLT, which did not remain statistically significant after FDR correction.

Cortical mean diffusivity group comparisons

Patients with iRBD showed three clusters of increased cMD, two in the right and one in the left hemisphere, compared to HC (Fig. 1).

In the right hemisphere, patients showed increased cMD in a rostral cluster with its peak in the rostral middle frontal gyrus (1797.38 mm^2, $x = 27.3$, $y = 44.5$, $z = 11.7$, $p < 0.001$). A caudal cluster was also identified, with its peak in the lateral occipital cortex (10,045.26 mm^2, $x = 10.4$, $y = -95.1$, $z = 12.6$, $p < 0.001$), including the inferior, and middle temporal gyri, superior parietal lobule, precuneus, cuneus, pericalcarine cortex, lingual, and fusiform gyri.

In the left hemisphere, patients showed increased cMD in a caudal cluster, with its peak in the pericalcarine cortex (5581.79 mm^2, $x = -14.7$, $y = -72.2$, $z = 14.3$, $p < 0.001$), including the fusiform and lingual gyri, cuneus, superior parietal lobule, lateral occipital cortex, middle and inferior temporal gyri.

Cortical thickness group comparisons

Patients with iRBD showed one caudal-medial cluster of cortical thinning in the whole brain compared to HC, in the right hemisphere (Fig. 2).

This cluster had its peak in the parahippocampal gyrus (884.67 mm^2, $x = 32.1$, $y = -36.3$, $z = -8.6$, $p = 0.001$), including the fusiform and lingual gyri.

For additional information, the overlap of both surface-based approach maps showing moderate to high effect sizes ($d > 0.5$) without the significant cluster restriction is represented in Supplementary Fig. 1. Moreover, age- and sex-controlled cMD and CTh results are presented in Supplementary Table 3, with a cluster-defining threshold set at 2.0 ($p < 0.01$) in both directions (abs).

Correlations between neuroimaging outcomes and clinical features

Changes in cMD in patients with iRBD positively correlated with age at iRBD onset, iRBD duration, MDS-UPDRS part III, and apathy. Also, changes in cMD in patients with iRBD positively correlated with dominant and non-dominant GPT, and negatively correlated with SDMT (Fig. 3A). Changes in CTh negatively correlated with disease duration (Fig. 3B). Correlational results involving dominant and non-dominant GPT remained statistically significant after removing participants with scores 2 standard deviations above or below the mean. Correlations between iRBD duration and MDS-UPDRS part III with cMD in the right rostral middle frontal survived FDR correction. Additionally, correlations between iRBD duration and CTh in the right parahippocampal cortex also survived FDR correction.

Although other neuropsychological variables showed statistically significant differences between groups, no additional correlations with cMD or CTh were found (Supplementary Table 4).

Discussion

This is the first study to demonstrate the usefulness of cMD in detecting subtle cortical microstructural changes throughout the entire brain in the early stages of LB diseases, with an extensive pattern of rostral and caudal alterations. These changes are associated with clinical features and neuropsychological performance of the patients with iRBD at high risk of phenoconversion to alpha-synucleinopathies. Microstructural changes are more pronounced than CTh measures.

cMD provides insights into cortical microstructural integrity and potentially reflects damage to dendrites or cellular membranes, leading to

Table 1 | Sociodemographic and clinical characteristics of the participants

	N	iRBD	HC	Statistics	p_{FDR}	Effect size
Age, years	36/29	71.81 (6.63)	69.86 (6.28)	-1.203^{St}	0.253	
Sex, male (%)	36/29	30 (83.33%)	18 (62.07%)	$2.740^{\times 2}$	0.127	
Education, years	36/29	12.39 (5.43)	15.00 (4.31)	2.108^{St}	0.063	
Education level	35/28	-	-	$5.625^{\times 2}$	0.155	
Literary skills	-	4 (11.43%)	0 (0.00%)	-	-	
Primary	-	6 (17.14%)	3 (10.71%)	-	-	
Secondary	-	12 (34.29%)	8 (28.57%)	-	-	
Post-secondary	-	13 (37.14%)	17 (60.71%)	-	-	
Age at RBD onset (years)	36/-	68.71 (6.42)	-	-	-	
RBD duration (years)	36/-	3.74 (4.40)	-	-	-	
Abnormal DaTSCAN[a] (%)	34/-	25 (73.53)	-	-	-	
MDS-UPDRS part III	33/-	1.36 (1.89)	-	-	-	
MCI (%)	36/29	13 (36.11)	6 (20.69)	$1.176^{\times 2}$	0.278	
MMSE	36/29	29.00 (1.00)*	30.00 (1.00)*	-2.976^{BM}	**0.008**	0.849
Vocabulary (WAIS-IV)	36/29	34.50 (10.25)*	39.00 (7.00)*	650.500^{U}	0.127	
NMS	34/29	7.50 (5.00)*	3.00 (2.00)*	5.201^{BM}	**<0.001**	1.478
AS	34/29	12.50 (6.44)	7.10 (4.37)	-3.940^{Wt}	**0.001**	0.967
BDI-II	34/29	7.00 (7.25)*	2.00 (5.00)*	3.085^{BM}	**0.007**	0.901
NPI	35/29	6.00 (14.00)*	0.00 (4.00)*	5.024^{BM}	**<0.001**	1.347
UPSIT	36/27	18.39 (6.28)	27.93 (5.80)	6.162^{St}	**<0.001**	1.569

Values denote mean (SD), median (IQR)*, or numbers (frequencies). Bold values denote statistically significant differences between groups ($p < 0.05$, FDR-corrected). Statistical tests used: Chi-Squared test$^{\times 2}$, Student's *t*-testSt, Welch's *t*-test^{Wt}, Mann–Whitney's U^{u}, Brunner-Munzel test^{BM}. Effect size: Cohen's *d* (continuous variables).

AS Starkstein Apathy Scale, *BDI-II* Beck's Depression Inventory-II, *HC* healthy controls, *iRBD* isolated REM sleep behavior disorder, *MCI* mild cognitive impairment, *MDS-UPDRS* Movement Disorder Society Unified Parkinson's Disease Rating Scale, *MMSE* Mini-Mental State Examination, *NMS* Non-Motor Symptoms questionnaire, *NPI* Neuropsychiatric Inventory, *RBD-I* Innsbruck REM Sleep Behavior Disorder Inventory, *UPSIT* University of Pennsylvania Smell Identification Test, *WAIS-IV* Wechsler's Adult Intelligence Scale-IV.

[a] Abnormal DaTSCAN: <65% normal, 2 SD below mean.

less restricted water diffusion within the gray matter[32]. As far as we know, it has not been studied in patients with iRBD. Previous studies revealed increased cMD in patients with PD compared to HC cross-sectionally[48] and longitudinally[46]. Additionally, increased cMD has been linked to poorer global cognition and higher depression and apathy symptoms in PD[48], and has been associated with biological markers of neurodegeneration[45,47]. Recently, our group studied CTh and cMD in patients with PD and probable/not probable RBD[49]. Patients with PD and probable RBD showed a bilateral caudal pattern with larger effect sizes and higher cMD than HC. Additionally, these patients showed rostral and caudal increased cMD bilaterally compared to patients with PD without probable RBD. Notably, the pattern of cMD alterations between PD patients with and without probable RBD was similar to that found in iRBD in the current study. This pattern primarily involved medial and lateral caudal regions, including the superior parietal cortex, precuneus, cuneus, pericalcarine, and lateral occipital cortices. Additionally, there were significant similarities in the occipitotemporal regions, encompassing the lingual, fusiform, and middle temporal gyri. Unfortunately, the current sample could not be compared with the previously analyzed PD and probable RBD samples due to differences in acquisition sequences.

Consistent with our findings, previous studies underscore the superior usefulness of cMD in detecting cortical microstructural alterations during the prodromal stages and clinical subtypes of various neurodegenerative diseases. A prior study identified cortico-microstructural alterations in different preclinical stages of AD compared to HC[39]. Furthermore, previous studies showed particular effectiveness in distinguishing patterns of cerebral microstructural changes in early and late preclinical stages of familial autosomal dominant AD mutation carriers[41], as well as in presymptomatic mutation carriers[37,50], compared to HC. Some cited studies, conducted in parallel with CTh, showed fewer cortical macrostructural than microstructural changes[34,41,46]. Two of them reported an overlap between the results of cMD and CTh[34,41]. In our results, the effect size maps of cMD and CTh showed a subjacent cortical thinning overlapping with increased cMD in the right lateral occipital cortex, inferior parietal lobule, precuneus, and rostral middle frontal gyrus, as well as in the left pericalcarine cortex and cuneus. This could suggest that microstructural changes precede macrostructural atrophy.

The precise physiopathological mechanisms underlying microstructural changes in the cortex associated with iRBD are not yet fully understood. The pathological role of the presence of Lewy-type alpha-synucleinopathy[51] might lead to a neurodegenerative process characterized by intracellular disorganization, neuronal damage, and progressive neural loss. A recent study using advanced imaging transcriptomics and spatial mapping indicated that mitochondrial dysfunction and macroautophagy are key drivers of cortical alterations in iRBD[52]. Histopathological studies identified different patterns of alpha-synuclein burden in cortical and subcortical regions associated with the symptomatology heterogeneity of LB diseases[53]. These changes could collapse water diffusion barriers, increasing extracellular water in the cortex, and consequently, cMD within vulnerable regions[33,50]. Other studies have demonstrated the relationship between cMD and neurodegeneration biomarkers, such as tau deposition in older adults[54], and in amyloid-β positive adults with MCI and dementia[55], serum neurofilament light chain levels[45], and homocysteine levels[47] in PD, as well as amyloid-β deposition in patients with MCI[56]. Considering the significant delay between the formation of protein aggregates and the onset of clinical symptoms[57,58], along with the presence of co-pathological proteins in the neural tissue of patients with iRBD[22], cMD emerges as a highly sensitive technique for detecting microstructural brain changes before macrostructural atrophy becomes evident in neuroimaging.

Table 2 | Neuropsychological performance of the participants without covariables

	N	iRBD	HC	Statistics	p_{FDR}	Effect size
Attention						
Digits forward span (WAIS-IV)	36/29	5.00 (2.00)*	6.00 (2.00)*	748.000^{U}	**0.013**	2.054
TMT part A	36/29	44.00 (25.00)*	38.00 (18.00)*	1.382^{BM}	0.198	0.409
Language						
Similarities (WAIS-IV)	36/29	19.28 (5.68)	22.41 (4.96)	2.340^{St}	**0.047**	0.584
BNT	36/29	13.00 (1.00)*	14.00 (2.00)*	667.500^{U}	0.077	1.663
Processing speed						
SDMT	36/29	39.72 (11.97)	50.62 (10.57)	3.843^{St}	**0.007**	0.959
Stroop Word	36/29	85.50 (17.01)	97.86 (18.98)	2.766^{St}	**0.024**	0.690
Stroop Color	36/29	53.75 (12.99)	61.21 (12.52)	2.338^{St}	**0.047**	0.583
Executive functions						
Semantic fluency (animals)	36/29	18.00 (5.25)*	22.00 (4.00)*	-3.344^{BM}	**0.011**	0.958
Phonetic fluency (letter P)	36/29	13.06 (4.72)	15.48 (4.65)	2.075^{St}	0.075	0.518
Stroop Word-color	36/29	29.36 (10.49)	34.14 (10.70)	1.808^{St}	0.102	0.451
Digits backward span (WAIS-IV)	36/29	4.00 (2.00)*	4.00 (1.00)*	630.500^{U}	0.167	1.515
TMT part B	29/28	107.00 (49.00)*	81.00 (58.75)*	1.627^{BM}	0.140	0.508
Memory						
RAVLT total	36/29	38.58 (10.14)	43.83 (8.62)	2.214^{St}	0.058	0.553
RAVLT delayed recall	36/29	7.53 (3.33)	9.07 (3.04)	1.928^{St}	0.090	0.481
RAVLT false recognition	36/29	1.00 (1.00)*	0.00 (1.00)*	2.731^{BM}	**0.024**	0.742
RMT-F	36/28	40.50 (6.69)	40.36 (5.57)	-0.091^{St}	0.928	0.023
Visuospatial/visuoperceptual abilities						
Clock copying test	36/29	14.00 (1.00)*	15.00 (1.00)*	-2.388^{BM}	**0.047**	0.622
JLO	36/29	23.00 (5.25)*	25.00 (7.00)*	-1.810^{BM}	0.102	0.529
BFRT-short	36/29	22.00 (2.08)	22.48 (2.31)	0.866^{Yt}	0.430	0.431
FM-100 Error score	34/24	166.00 (124.00)*	164.00 (67.00)*	0.805^{BM}	0.444	0.250
Manual dexterity						
Dominant GPT, seconds	36/25	95.00 (22.00)*	78.00 (29.00)*	3.506^{BM}	**0.011**	1.165
Non-dominant GPT, seconds	35/25	115.00 (36.50)*	90.00 (22.00)*	3.107^{BM}	**0.014**	0.952
Social cognition						
RMET	35/29	19.66 (4.92)	22.76 (3.18)	3.039^{Wt}	**0.014**	0.734

Values denote mean (SD), median (IQR)*, or numbers (frequencies). Bold values denote statistically significant differences between groups ($p < 0.05$, FDR-corrected). Statistical tests used: Student's *t*-testSt, Welch's *t*-test^{Wt}, Yuen's t-test^{Yt}, Mann–Whitney's U^{u}, Brunner-Munzel test^{BM}. Effect size: Cohen's *d*.

BFRT Benton Facial Recognition Test, *BNT* Boston Naming Test, *GPT* Grooved Pegboard Test, *HC* healthy controls, *iRBD* isolated REM sleep behavior disorder, *JLO* Judgment of Line Orientation, *RAVLT* Rey-Auditory Verbal Learning Test, *RMET* Reading the Mind in the Eyes Test, *RMT-F* Warrington Recognition Memory Test for Faces, *SDMT* Symbol Digit Modalities Test, *TMT* Trail Making Test, *WAIS-IV* Wechsler's Adult Intelligence Scale-IV.

The absence of cMD studies in iRBD leads us to compare our findings with structural MRI studies that used other surface-based approaches. Prior CTh studies in video-polysomnography-confirmed iRBD patients without cognitive or motor comorbidities described primarily rostral brain atrophy, including the superior[24,25,28], inferior[27], and medial[24,26] frontal regions, as well as the orbitofrontal[25], cingulate[24,25], paracingulate[24], precentral[25,26,28] and paracentral[26,28] cortices. These findings were aligned with our cMD results involving the rostral middle frontal gyrus. Surprisingly, CTh analysis in our sample did not detect rostral macrostructural alterations, likely due to differences in sample size[25,26], mean age[24–27], cognitive status of patients[24,25], and methodological approaches[24–28]. A previous study found that cMD exhibited particularly high sensitivity in frontal and insular regions in patients with AD[41]. The detection of rostral abnormalities using cMD, as opposed to CTh, might be attributed to each region's different degeneration time points. The overlapping map of CTh and cMD effect sizes, without significant cluster restriction, might back up this statement, showing moderate subjacent cortical thinning in patients with iRBD in inferior, middle, and superior lateral and medial, as well as paracingulate regions.

Our results also showed evident increased cMD in patients in the caudal regions bilaterally. In iRBD, cortical thinning has also been consistently reported in the postcentral[28,29], superior[28] and inferior parietal[29], supramarginal[29], cuneus[27], superior[27] and lateral occipital[28–30], fusiform[24,28], lingual[24,28], superior and middle temporal[27] cortices compared to HC. Similarly to our findings, an extensive CTh multicenter study in iRBD, including patients with MoCA scores below 25, reported widespread rostral and caudal alterations[59]. Likewise, a prior study by our group, with a slightly smaller sample size but comparable sociodemographic characteristics, identified cortical thinning involving rostral and caudal regions, closely aligning with our cMD findings[28]. Probably, the inclusion of elderly patients increased the probability of including more patients at high risk of conversion[10], bringing their cortico-structural results similar to ours.

The extensive pattern of caudal and rostral microstructural alterations observed may reflect the high sensitivity of cMD in detecting a more widespread pattern of neurodegeneration compared to CTh. Our results in the between-group comparisons, together with the effect size maps (Supplementary Fig. 1), suggest that the subjacent cortical thinning evidenced in

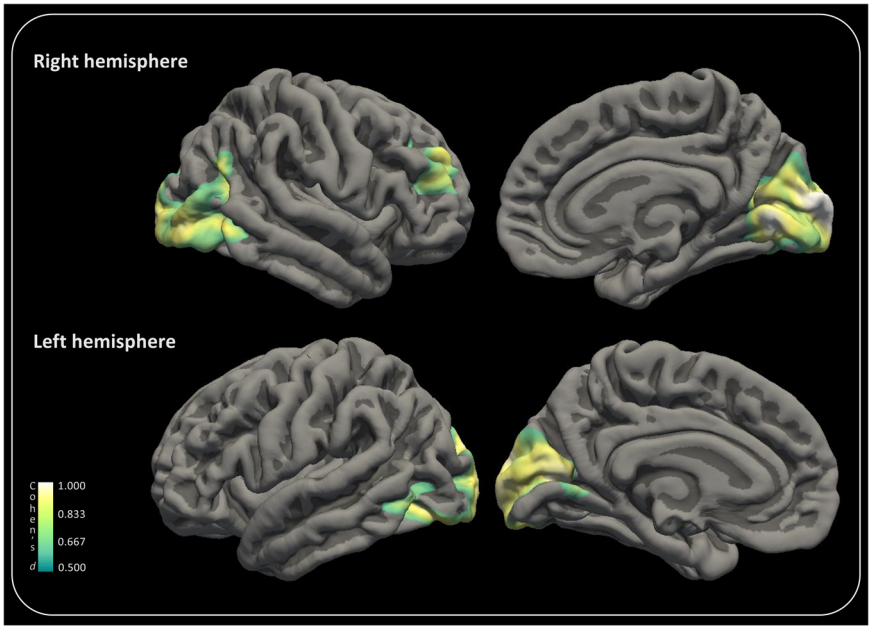

Fig. 1 | Cortical mean diffusivity comparisons between iRBD and HC. Patients with iRBD showed increased cMD in comparison with HC. Only clusters that survived cluster-extend Monte Carlo corrections for multiple comparisons ($p < 0.01$, FWE-corrected) are represented, with effect sizes (Cohen's $d > 0.5$) restricted to the significant clusters.

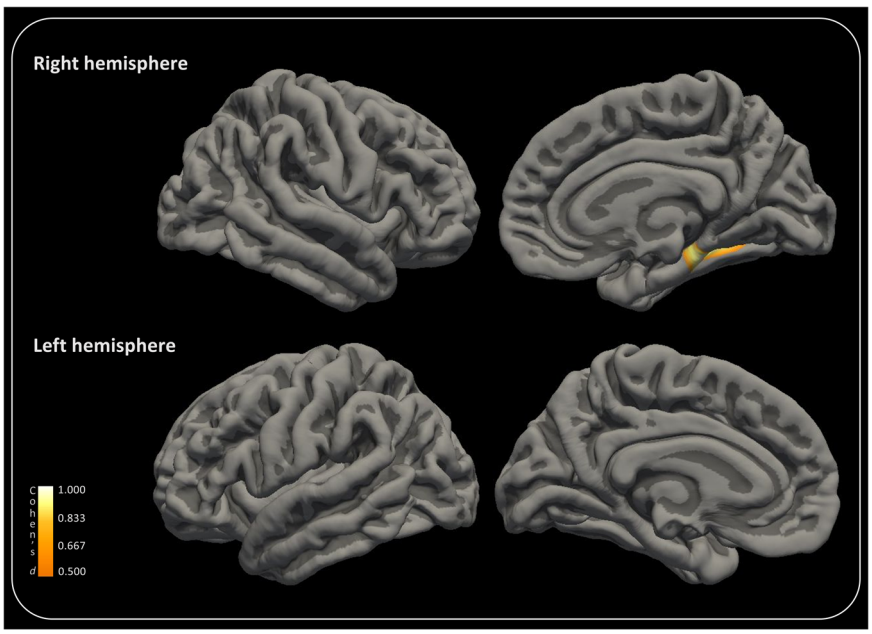

Fig. 2 | Cortical thickness comparisons between iRBD and HC. Patients with iRBD showed cortical thinning in comparison with HC. Only clusters that survived cluster-extend Monte Carlo corrections for multiple comparisons ($p < 0.01$, FWE-corrected) are represented, with effect sizes (Cohen's $d > 0.5$) restricted to the significant clusters.

some regions showing microstructural alterations may reflect the temporal sequence of neurodegeneration leading up to phenoconversion in our sample. The present results may indicate a possible trajectory of neurodegeneration towards a more severe phenotype of LB diseases, characterized by more prominent cortical caudal involvement[31]. However, further clustering studies with longitudinal follow-ups are needed to determine the phenotypic conversion.

Previous iRBD studies have shown an early asymmetric vulnerability to cerebral changes of the left hemisphere over the right hemisphere[60,61]. In our analyses, the between-group comparisons might suggest an asymmetric pattern with greater alterations in the right hemisphere, although the effect size maps indicate bilateral involvement.

Furthermore, this is the first study describing associations between cMD and clinical features in patients with iRBD at high risk of phenoconversion. In the current study, longer disease duration and older age at onset have been associated with increased cMD. Bringing our findings in line with other surface-based approaches, one previous study with a moderately large sample described correlations between longer disease duration and cortical thinning in frontal and occipital regions among patients with iRBD[25]. Also, late iRBD onset was associated with thinning in the precuneus and lateral occipital cortices in a longitudinal study[31]. Overall, these results suggest more pronounced cortical atrophy patterns in patients with later onset and longer disease duration. Remarkably, the probability of patients with iRBD developing a synucleinopathy increases over time[9,25,62].

Bearing in mind the correlations between cortico-structural alterations and neuropsychological performance, our study showed associations between increased cMD and protracted time performing GPT, in both hands, in the rostral middle frontal, lateral occipital and pericalcarine regions, along with increased cMD and low performance in SDMT in the lateral occipital cortex cluster. Our findings may extend previous evidence

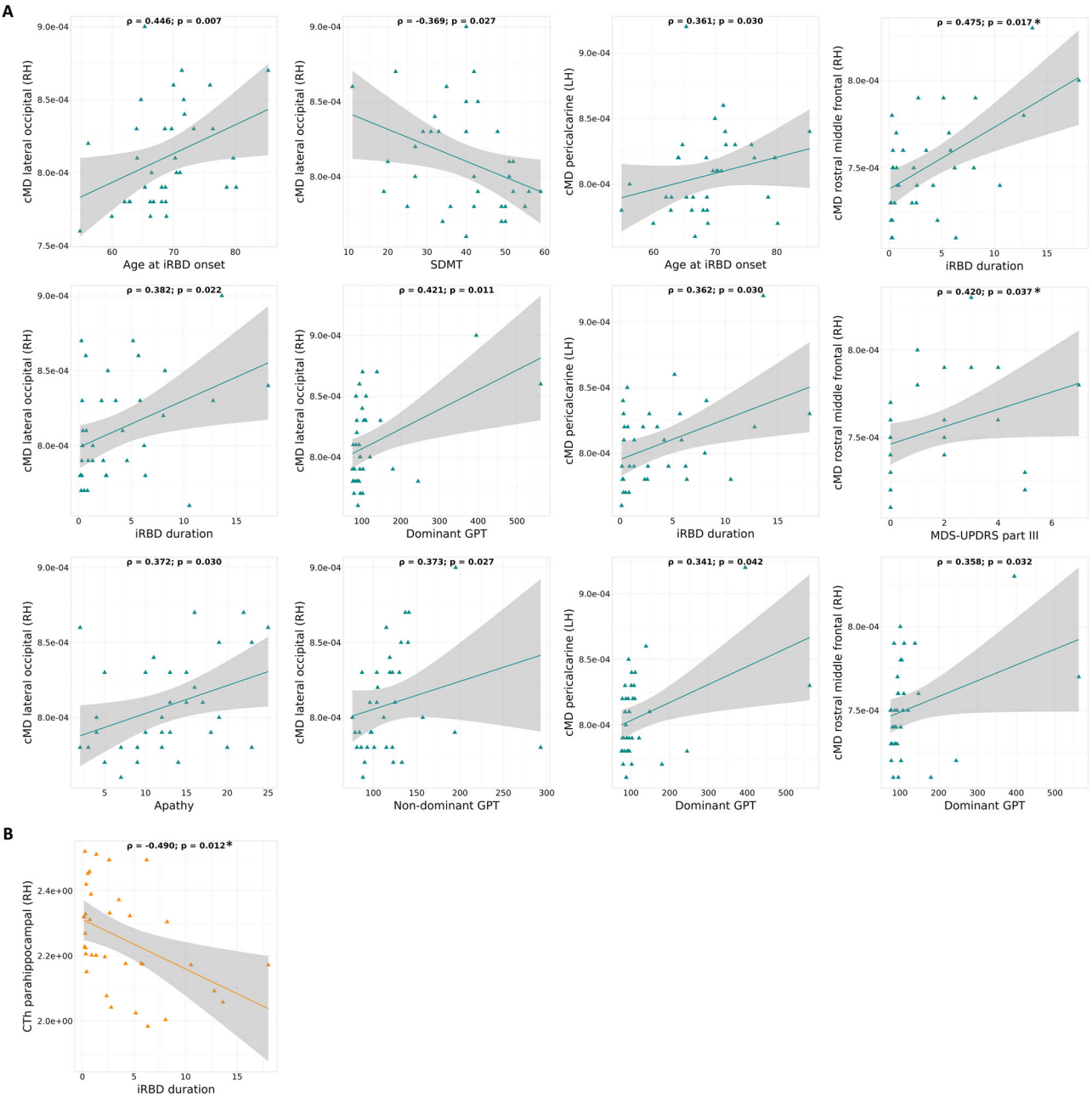

Fig. 3 | Correlations between cMD and CTh and clinical/neuropsychological features in patients with iRBD. A Correlations between cMD and clinical/neuropsychological features in patients with iRBD. **B** Correlation between CTh and disease duration in patients with iRBD. *Correlations that survived FDR correction. CTh cortical thickness, cMD cortical mean diffusivity, GPT Grooved pegboard test, iRBD isolated REM sleep behavior disorder, SDMT symbol-digit modalities test.

on the usefulness of SDMT as a sensitive neuropsychological measure associated with caudal cortical abnormalities in iRBD[60], and caudal cortical atrophy in overt alpha-synucleinopathies[63]. No previous studies have explored the relationship between cMD and cognitive performance in iRBD. However, evidence in PD showed associations between global cognition through the Parkinson's disease Cognitive Rating Scale and cMD in parahippocampal, entorhinal, superior frontal, rostral, and caudal middle frontal, superior temporal, inferior parietal, and supramarginal gyri, along with the banks of superior temporal sulcus[48]. These findings may indicate that, to some extent, the cortical microstructural alterations in the rostral middle frontal gyrus may be relevant for cognitive impairment in alpha-synucleopathies progression, although further research is needed to confirm these associations.

The heterogeneous symptomatology and prolonged latency of iRBD make identifying reliable biomarkers difficult. The challenges of long-term studies confer a higher interest in focusing on the nearest phenoconversion time points[12,14], where concomitant symptoms are more prevalent[64] and phenoconversion rates per year are more elevated. The risk of phenoconversion to an overt neurodegenerative syndrome increases drastically in the later stages of iRBD[6,9], which could help identify potential predictors of phenoconversion. Patients with iRBD at high risk of conversion to fully developed neurodegenerative diseases could be ideal targets for neuroprotective clinical trials aimed at slowing or preventing the onset of LB diseases[12,14].

Considering the limitations and strengths of this study is crucial for understanding the results. The HC group did not undergo video-polysomnography to rule out iRBD, although a sleep interview revealed that RBD was not suspected based on the clinical history. This study did not include biomarkers to exclude other preclinical neurodegenerative disorders. Accounting for the strengths of this study, to our knowledge, this is

the first study to assess cortical microstructural alterations using cMD in patients with video-polysomnography-proven iRBD at high risk of conversion to LB diseases, compared to well-matched HC. The study includes a thorough multiple-domain neuropsychological assessment, including the evaluation of non-motor symptoms and olfactory function. Other strengths include the implementation of a multimodal neuroimaging approach of validated surface-based techniques and the computation of Cohen's *d* effect sizes. Moreover, the computation of cMD was made through an improved method that overcomes previous methodological concerns[34]. Further studies should replicate these findings with larger, well-matched samples to validate our results. Future longitudinal multimodal studies including patients with iRBD at low risk are needed to compare cortical macro- and microstructural changes over time and to evaluate the suitability of cMD as an imaging biomarker for progression in alpha-synucleopathies. Moreover, studies with larger cohorts and advanced clustering techniques could allow to further explore inter-individual variability in cMD alterations in iRBD.

To summarize, our findings revealed an extensive pattern of rostral and caudal cortical microstructural involvement in patients with iRBD at high risk of phenoconversion, associated with clinical features, subtle motor dysfunctions, and processing speed. This study highlights the usefulness of cMD over CTh in detecting subtle cortico-structural alterations during the prodromal stages of LB diseases. Consequently, cMD could have potential as a promising neuroimaging biomarker to identify at-risk populations to phenoconvert.

Methods

Participants

Participants were recruited from the Sleep Unit of the Neurology Service at the Hospital Clínic, located in Barcelona (Catalonia, Spain). The total sample comprised 73 participants, 44 patients with iRBD confirmed by video-polysomnography and 29 age- and sex-matched healthy controls (HC).

The inclusion criteria for patients included: (1) video-polysomnographic demonstration of dream-enacting behaviors and absence of atonia during REM sleep, (2) high risk of conversion to alpha-synucleinopathies according to the MDS criteria for prodromal PD[13], (3) no motor complaints at the recruitment time, (4) unremarkable neurological examination, and (5) no temporal association between the introduction/withdrawal of medication and the estimated iRBD onset[21].

The exclusion criteria for patients were: (1) the presence of dementia according to the MDS criteria[65], (2) scores below 25 in the Mini-Mental State Examination (MMSE)[66], (3) severe psychiatric or neurological comorbidities, (4) claustrophobia, (5) remarkable pathological MRI findings, and (6) MRI artifacts. The exclusion criteria for HC included: (1) scores below 25 in the MMSE, and (2) self-reported RBD symptomatology. History of nasal bone fracture, polyps, rhinitis, and upper respiratory tract infections 2 weeks before testing were specific exclusion criteria for the olfactory function assessment for all the participants.

The final sample, after applying the exclusion criteria, is reported in the "Results" section.

The present study was approved by the Bioethics Committee of the University of Barcelona (IRB00003099). All participants signed written informed consent.

Clinical and neuropsychological assessment

Relevant sociodemographic information was registered for all participants, and clinical features for the patients. These data included the date of diagnosis and duration of iRBD, current medication intake (Supplementary Table 1), and severity of motor symptoms through part III of the Unified Parkinson's Disease Rating Scale (UPDRS-III)[67]. Also, neuropsychiatric and pathological-related non-motor symptoms were assessed using the Cummings Neuropsychiatric Inventory (NPI)[68], Beck Depression Inventory 2nd edition (BDI-II)[69], Starkstein Apathy Scale (AS)[70], Non-Motor Symptoms (NMS) questionnaire for Parkinson's disease[71].

Furthermore, all participants underwent a comprehensive neuropsychological assessment. The MMSE was used to evaluate global cognition, and the Vocabulary subtest of the WAIS-IV to estimate premorbid intelligence. The specific neuropsychological assessment included: (1) Digits forward subtest (WAIS-IV), and Trail Making Test (TMT) part A to evaluate attention, (2) Similarities subtest (WAIS-IV), and Boston Naming Test (BNT) to assess language, (3) Symbol Digit Modalities Test (SDMT) oral version, and Stroop word and the Stroop color subtests to assess processing speed, (4) semantic (animals) and phonetic (letter "P") fluency tests, Stroop word-color subtest, Digits backward subtest (WAIS-IV), and TMT part B to evaluate executive functions, (5) Reading the Mind in the Eyes Test (RMET) to assess social cognition, (6) Rey's Auditory Verbal Learning Test (RAVLT), Warrington Recognition Memory Test for Faces (RMT-F) to evaluate memory, (7) clock copying test, Benton's Judgment of Line Orientation (JLO), short version of Benton's Facial Recognition Test, Farnsworth-Munsell 100-Hue test (FM-100) to assess visuospatial/visuoperceptual abilities, (8) Grooved Pegboard test (GPT) to evaluate manual dexterity, and (9) University of Pennsylvania Smell Identification Test with 40 items (UPSIT-40) to assess olfactory function.

To assess mild cognitive impairment (MCI) based on psychometric measures, Z-scores and expected Z-scores adjusted for age, sex, and years of education were calculated on each neuropsychological test through a multiple regression analysis performed in the HC group. Participants with two or more impaired neuropsychological tests (<1.5 SD) within a single domain were classified as having MCI[72].

The high-risk characterization was conducted using the MDS criteria for prodromal PD[13]. The percentage was calculated using an evidence-based and validated Bayesian classifier that integrates the following risk markers: male sex, pesticide and solvent exposure, non-use of caffeine, smoking, family history of PD, type-II diabetes mellitus, physical inactivity, polysomnography-proven RBD, abnormal dopaminergic imaging, UPDRS-III > 3, olfactory loss, constipation, excessive daytime somnolence, neurogenic or symptomatic orthostatic hypotension, urinary and erectile dysfunction, depression and global cognitive deficit. Each marker's likelihood ratio was used to compute the overall probability of prodromal PD. Only patients with RBD with a probability higher than 80% were considered at high risk of conversion to alpha-synucleinopathies.

MRI acquisition and preprocessing

MRI was performed on a 3 T scanner (Siemens Magnetom Prisma) at the Centre de Diagnostic per la Imatge of the Hospital Clínic de Barcelona (Catalonia, Spain). The scanning protocol included high-resolution 3-dimensional T1-weighted images (TR = 2400 ms, TE = 2.22 ms, TI = 1000 ms, voxel size = 0.8 mm isotropic voxel) and two sets of multi-band spin-echo DWI with opposite phase encoding directions. Also, T2-weighted images and FLAIR sequences were acquired to evaluate the effects of aging and microvascular lesions visually. For detailed information about the MRI acquisition parameters, see Supplementary Table 2.

T1-weighted MRI processing

The automated FreeSurfer stream version 6.0, available at https://surfer.nmr.mgh.harvard.edu/, was used to estimate cortical thickness (CTh). The procedures in FreeSurfer included removal of non-brain data, registration to Talairach space, intensity normalization, and tessellation of the gray matter and white matter boundaries, automated topology correction, and accurate surface deformation following intensity gradients to identify tissue borders. Cortical thickness was calculated as the distance between the white and gray matter surfaces at each vertex of the reconstructed cortical mantle (https://freesurfer.net/fswiki/FreeSurferMethodsCitation). Results for each subject were visually inspected, and the befitting manual corrections were also performed to ensure the accuracy of registration, skull stripping, segmentation, and cortical surface reconstruction (https://surfer.nmr.mgh.harvard.edu/fswiki/FsTutorial/TroubleshootingData).

Diffusion-weighted MRI processing

The FMRIB's Diffusion Toolbox (FDT) software from FSL (https://fsl.fmrib.ox.ac.uk/fsl/docs/#/) was used to analyze diffusion-weighted MRI

images through a diffusion tensor imaging (DTI) approach. Only b-value = 1500 s/mm^2 was used to calculate tensor metrics due to the issues about non-Gaussian diffusion at high b-values and the estimation of tensor metrics from multi-shell data[73]. The processing started with the estimation and correction for susceptibility-induced distortions[74] (TOPUP, https://fsl.fmrib.ox.ac.uk/fsl/docs/#/diffusion/topup/index), the brain extraction using the Brain Extraction Tool[75] (BET, https://fsl.fmrib.ox.ac.uk/fsl/docs/#/structural/bet), and distortion correction using EDDY[76] (https://fsl.fmrib.ox.ac.uk/fsl/docs/#/diffusion/eddy/index) that simultaneously corrects for eddy currents and subject motion. These processing tools face common challenges of echo-planar imaging (EPI) sequences[77]. Individual mean diffusivity (MD) maps were obtained using a diffusion model fit (DTIFIT, https://fsl.fmrib.ox.ac.uk/fsl/docs/#/diffusion/dtifit).

Cortical mean diffusivity processing

The FMRIB's Diffusion Toolbox (FDT) software from FSL and the FreeSurfer package, version 6.0, were also implemented to process cortical diffusion MRI data using a surface-based DTI approach[34]. The MD volumes were co-registered to the anatomic subject space, projected to the surface, normalized using a spherical registration to the Freesurfer standard template, and smoothed. The diffusion images were corrected for motion effects, skull-stripped, DTI tensor fitted, and projected to the brain surface. Before further analyses, a Gaussian kernel of 15 mm FWHM was applied to the subjects' MD surface maps. Finally, the surface MD maps were used for the statistical analyses.

Statistical analyses

The statistical analyses of sociodemographic, neuropsychological, and clinical data were performed using R Statistical Software, version 4.3.1 (R Core Team 2023, https://www.r-project.org/). The sample size, the presence of outliers, and the normality and equal variances assumptions were considered to decide the most suitable statistical test for each variable. Shapiro–Wilk and Levene's tests assessed normality and variance homogeneity, respectively. Depending on the data distribution, the Student's *t*-test, Welch's *t*-test, Mann–Whitney's U test, Yuen's *t*-test, or Brunner–Munzel test was applied for between-group comparisons. The Student's *t*-test was conducted when the data met the normality and equal variances assumptions without outliers. The Welch's *t*-test was performed when the data had unequal variances. The Mann–Whitney test was used when the variables violated the normality assumption without outliers. Yuen's *t*-test or Brunner-Munzel's test was conducted when the variables presented outliers with or without data normally distributed, respectively. Categorical variables were analyzed through Pearson's chi-squared test.

The effect size was calculated for each variable depending on the statistical test of group comparison implemented, using Cohen's *d*, trimmed mean effect size, Pearson's *r*, or probability of superiority when necessary. Results were converted to Cohen's *d* posteriorly, to homogenize this metric. Pearson's (r) or Spearman's (ρ) correlations, depending on the normality of the data, were performed to assess the associations between statistically significant neuroimaging and neuropsychological or clinical variables in the between-group comparisons. The statistical threshold was set at $p < 0.05$, two-tailed. All the results were corrected by False Discovery Rate (FDR) using the Benjamini–Hochberg method.

Between-group cMD and CTh analyses were performed through a two-class vertex-wise general linear model (GLM) using FreeSurfer, version 6.0, with a cluster-defining threshold set at 2.0 ($p < 0.01$) in both directions (abs). In both imaging analyses, cluster-extend corrections for multiple comparisons were tested through the Monte Carlo simulation with 10,000 iterations implemented in FreeSurfer. Only the clusters that survived family-wise error (FWE) ($p < 0.01$) were reported. The mean CTh and cMD of each significant cluster from the between-group comparisons were calculated for each participant, and these values were used to perform correlational analyses. Furthermore, vertex-wise Cohen's *d* effect sizes were computed for cMD and CTh, limiting effect size results to the statistically significant regions obtained in the intergroup comparison analyses to represent the effect size of the topographical differences between HC and iRBD. Only moderate to high effect sizes were considered ($d > 0.5$).

Data availability

The datasets generated and/or analyzed during the current study are not publicly available due to privacy or ethical restrictions, but the de-identified data that support the findings of this study are available from the corresponding author upon reasonable request.

Received: 11 February 2025; Accepted: 16 June 2025;
Published online: 03 July 2025

References

1. Iranzo, A. et al. Rapid-eye-movement sleep behaviour disorder as an early marker for a neurodegenerative disorder: a descriptive study. *Lancet Neurol.* **5**, 572–577 (2006).
2. Sateia, M. J. International classification of sleep disorders—third edition highlights and modifications. *Chest* **146**, 1387–1394 (2014).
3. Berg, D. et al. MDS research criteria for prodromal Parkinson's disease. *Mov. Disord.* **30**, 1600–1611 (2015).
4. McKeith, I. G. et al. Research criteria for the diagnosis of prodromal dementia with Lewy bodies. *Neurology* **94**, 743–755 (2020).
5. Xia, C. & Postuma, R. B. Diagnosing multiple system atrophy at the prodromal stage. *Clin. Auton. Res.* **30**, 197–205 (2020).
6. Galbiati, A., Verga, L., Giora, E., Zucconi, M. & Ferini-Strambi, L. The risk of neurodegeneration in REM sleep behavior disorder: a systematic review and meta-analysis of longitudinal studies. *Sleep. Med. Rev.* **43**, 37–46 (2019).
7. Leitner, C. et al. Neuropsychological changes in isolated REM sleep behavior disorder: a systematic review and meta-analysis of cross-sectional and longitudinal studies. *Neuropsychol. Rev.* **34**, 41–66 (2024).
8. Schenck, C. H., Boeve, B. F. & Mahowald, M. W. Delayed emergence of a Parkinsonian disorder or dementia in 81% of older men initially diagnosed with idiopathic rapid eye movement sleep behavior disorder: a 16-year update on a previously reported series. *Sleep. Med.* **14**, 744–748 (2013).
9. Iranzo, A. et al. Neurodegenerative disorder risk in idiopathic REM sleep behavior disorder: study in 174 patients. *PLoS ONE* **9**, e89741 (2014).
10. Postuma, R. B., Gagnon, J.-F., Bertrand, J.-A., Marchand, D. G. & Montplaisir, J. Y. Parkinson risk in idiopathic REM sleep behavior disorder: preparing for neuroprotective trials. *Neurology* **84**, 1104–1113 (2015).
11. Iranzo, A. Sleep in neurodegenerative diseases. *Sleep. Med. Clin.* **11**, 1–18 (2016).
12. Iranzo, A., Santamaria, J. & Tolosa, E. Idiopathic rapid eye movement sleep behaviour disorder: diagnosis, management, and the need for neuroprotective interventions. *Lancet Neurol.* **15**, 405–419 (2016).
13. Heinzel, S. et al. Update of the MDS research criteria for prodromal Parkinson's disease. *Mov. Disord.* **34**, 1464–1470 (2019).
14. Postuma, R. B. Neuroprotective trials in REM sleep behavior disorder: the way forward becomes clearer. *Neurology* **99**, 19–25 (2022).
15. Joza, S. et al. Is REM sleep behavior disorder changing? Secular changes versus referral patterns. *Mov. Disord. Clin. Pract.* **10**, 1519–1524 (2023).
16. Fereshtehnejad, S. M. et al. Validation of the MDS research criteria for prodromal Parkinson's disease: longitudinal assessment in a REM sleep behavior disorder (RBD) cohort. *Mov. Disord.* **32**, 865–873 (2017).
17. Högl, B., Stefani, A. & Videnovic, A. Idiopathic REM sleep behaviour disorder and neurodegeneration—an update. *Nat. Rev. Neurol.* **14**, 40–56 (2018).
18. Miglis, M. G. et al. Biomarkers of conversion to α-synucleinopathy in isolated rapid-eye-movement sleep behaviour disorder. *Lancet Neurol.* **20**, 671–684 (2021).

19. Postuma, R. B. et al. Identifying prodromal Parkinson's disease: pre-motor disorders in Parkinson's disease. *Mov. Disord.* **27**, 617–626 (2012).
20. Mahlknecht, P., Marini, K., Werkmann, M., Poewe, W. & Seppi, K. Prodromal Parkinson's disease: hype or hope for disease-modification trials? *Transl. Neurodegener.* **11**, 11 (2022).
21. Boeve, B. F. REM sleep behavior disorder: updated review of the core features, the REM sleep behavior disorder-neurodegenerative disease association, evolving concepts, controversies, and future directions. *Ann. N. Y. Acad. Sci.* **1184**, 15–54 (2010).
22. Mayà, G. et al. Post-mortem neuropathology of idiopathic rapid eye movement sleep behaviour disorder: a case series. *Lancet Neurol.* **23**, 1238–1251 (2024).
23. Campabadal, A., Segura, B., Junque, C. & Iranzo, A. Structural and functional magnetic resonance imaging in isolated REM sleep behavior disorder: a systematic review of studies using neuroimaging software. *Sleep Med. Rev.* **59**, 101495 (2021).
24. Rahayel, S. et al. Patterns of cortical thinning in idiopathic rapid eye movement sleep behavior disorder. *Mov. Disord.* **30**, 680–687 (2015).
25. Rahayel, S. et al. Abnormal gray matter shape, thickness, and volume in the motor cortico-subcortical loop in idiopathic rapid eye movement sleep behavior disorder: association with clinical and motor features. *Cereb. Cortex* **28**, 658–671 (2018).
26. Rahayel, S. et al. Cortical and subcortical gray matter bases of cognitive deficits in REM sleep behavior disorder. *Neurology* **90**, E1759–E1770 (2018).
27. Park, G. et al. Static and dynamic brain morphological changes in isolated REM sleep behavior disorder compared to normal aging. *Front. Neurosci.* **18**, 1365307 (2024).
28. Campabadal, A. et al. Cortical gray matter and hippocampal atrophy in idiopathic rapid eye movement sleep behavior disorder. *Front. Neurol.* **10**, 312 (2019).
29. Pereira, J. B. et al. Cortical thinning in patients with REM sleep behavior disorder is associated with clinical progression. *NPJ Parkinsons Dis.* **5**, 7 (2019).
30. Chen, J. et al. Impaired ocular tracking and cortical atrophy in idiopathic rapid eye movement sleep behavior disorder. *Mov. Disord.* **37**, 972–982 (2022).
31. Campabadal, A. et al. Cortical gray matter progression in idiopathic REM sleep behavior disorder and its relation to cognitive decline. *Neuroimage Clin.* **28**, 102421 (2020).
32. Zarkali, A., Thomas, G. E. C., Zetterberg, H. & Weil, R. S. Neuroimaging and fluid biomarkers in Parkinson's disease in an era of targeted interventions. *Nat. Commun.* **15**, 5661 (2024).
33. Weston, P. S. J., Simpson, I. J. A., Ryan, N. S., Ourselin, S. & Fox, N. C. Diffusion imaging changes in grey matter in Alzheimer's disease: a potential marker of early neurodegeneration. *Alzheimers Res. Ther.* **7**, 47 (2015).
34. Montal, V. et al. Cortical microstructural changes along the Alzheimer's disease continuum. *Alzheimer's Dement.* **14**, 340–351 (2018).
35. Illán-Gala, I. et al. Cortical microstructure in the behavioural variant of frontotemporal dementia: looking beyond atrophy. *Brain* **142**, 1121–1133 (2019).
36. Sampedro, F. et al. Widespread increased diffusivity reveals early cortical degeneration in Huntington disease. *Am. J. Neuroradiol.* **40**, 1464–1468 (2019).
37. Vilaplana, E. et al. Cortical microstructural correlates of astrocytosis in autosomal-dominant Alzheimer disease. *Neurology* **94**, E2026–E2036 (2020).
38. Lee, P., Kim, H. R. & Jeong, Y. Detection of gray matter microstructural changes in Alzheimer's disease continuum using fiber orientation. *BMC Neurol.* **20**, 362 (2020).
39. Illán-Gala, I. et al. Cortical microstructure in the amyotrophic lateral sclerosis-frontotemporal dementia continuum. *Neurology* **95**, E2565–E2576 (2020).
40. Stock, B. et al. Distribution of cortical diffusion tensor imaging changes in multiple sclerosis. *Front. Physiol.* **11**, 116 (2020).
41. Montal, V. et al. Biphasic cortical macro- and microstructural changes in autosomal dominant Alzheimer's disease. *Alzheimer's Dement.* **17**, 618–628 (2021).
42. Sampedro, F. et al. Cortical microstructural correlates of plasma neurofilament light chain in Huntington's disease. *Parkinsonism Relat. Disord.* **85**, 91–94 (2021).
43. Solana, E. et al. Regional grey matter microstructural changes and volume loss according to disease duration in multiple sclerosis patients. *Sci. Rep.* **11**, 16805 (2021).
44. Illán-Gala, I. et al. Cortical microstructure in primary progressive aphasia: a multicenter study. *Alzheimers Res. Ther.* **14**, 27 (2022).
45. Sampedro, F. et al. Serum neurofilament light chain levels reflect cortical neurodegeneration in de novo Parkinson's disease. *Parkinsonism Relat. Disord.* **74**, 43–49 (2020).
46. Sampedro, F., Martínez-Horta, S., Marín-Lahoz, J., Pagonabarraga, J. & Kulisevsky, J. Longitudinal intracortical diffusivity changes in de-novo Parkinson's disease: a promising imaging biomarker. *Parkinsonism Relat. Disord.* **68**, 22–25 (2019).
47. Sampedro, F. et al. Increased homocysteine levels correlate with cortical structural damage in Parkinson's disease. *J. Neurol. Sci.* **434**, 120148 (2022).
48. Sampedro, F. et al. Cortical macro and microstructural correlates of cognitive and neuropsychiatric symptoms in Parkinson's disease. *Clin. Neurol. Neurosurg.* **224**, 107531 (2023).
49. Pardo, J. et al. Cortical macro- and microstructural changes in Parkinson's disease with probable rapid eye movement sleep behavior disorder. *Mov. Disord.* **39**, 814–824 (2024).
50. Weston, P. S. J. et al. Measuring cortical mean diffusivity to assess early microstructural cortical change in presymptomatic familial Alzheimer's disease. *Alzheimers Res. Ther.* **12**, 112 (2020).
51. Adler, C. H. & Beach, T. G. Neuropathological basis of nonmotor manifestations of Parkinson's disease. *Mov. Disord.* **31**, 1114–1119 (2016).
52. Rahayel, S. et al. Mitochondrial function-associated genes underlie cortical atrophy in prodromal synucleinopathies. *Brain* **146**, 3301–3318 (2023).
53. Colloby, S. J. et al. Patterns of tau, amyloid and synuclein pathology in ageing, Alzheimer's disease and synucleinopathies. *Brain* **148**, 1562–1576 (2025).
54. Rodriguez-Vieitez, E. et al. Association of cortical microstructure with amyloid-β and tau: impact on cognitive decline, neurodegeneration, and clinical progression in older adults. *Mol. Psychiatry* **26**, 7813–7822 (2021).
55. Sun, P. et al. Spatial and temporal patterns of cortical mean diffusivity in Alzheimer's disease and suspected non-Alzheimer's disease pathophysiology. *Alzheimers Dement.* **21**, 7048–7061 (2024).
56. Debatisse, J., Leng, F., Ashraf, A. & Edison, P. Cortical diffusivity, a biomarker for early neuronal damage, is associated with amyloid-β deposition: a pilot study. *Cells* **14**, 155 (2025).
57. Goedert, M., Falcon, B., Clavaguera, F. & Tolnay, M. Prion-like mechanisms in the pathogenesis of tauopathies and synucleinopathies. *Curr. Neurol. Neurosci. Rep.* **14**, 1–11 (2014).
58. Goedert, M., Masuda-Suzukake, M. & Falcon, B. Like prions: the propagation of aggregated tau and α-synuclein in neurodegeneration. *Brain* **140**, 266–278 (2017).
59. Rahayel, S. et al. Brain atrophy in prodromal synucleinopathy is shaped by structural connectivity and gene expression. *Brain* **145**, 3162–3178 (2022).
60. Campabadal, A. et al. Disruption of posterior brain functional connectivity and its relation to cognitive impairment in idiopathic REM sleep behavior disorder. *Neuroimage Clin.* **25**, 102138 (2020).

61. Iranzo, A. et al. Left-hemispheric predominance of nigrostriatal deficit in isolated REM sleep behavior disorder. *Neurology* **94**, E1605–E1613 (2020).
62. Postuma, R. B. et al. Risk factors for neurodegeneration in idiopathic rapid eye movement sleep behavior disorder: a multicenter study. *Ann. Neurol.* **77**, 830–839 (2015).
63. Garcia-Diaz, A. I. et al. Structural brain correlations of visuospatial and visuoperceptual tests in Parkinson's disease. *J. Int. Neuropsychol. Soc.* **24**, 33–44 (2018).
64. Fereshtehnejad, S.-M. et al. Evolution of prodromal Parkinson's disease and dementia with Lewy bodies: a prospective study. *Brain* **142**, 2051–2067 (2019).
65. Dubois, B. et al. Diagnostic procedures for Parkinson's disease dementia: recommendations from the Movement Disorder Society Task Force. *Mov. Disord.* **22**, 2314–2324 (2007).
66. Folstein, M. F., Folstein, S. E. & McHugh, P. R. "Mini-mental state": a practical method for grading the cognitive state of patients for the clinician. *J. Psychiatr. Res.* **12**, 189–198 (1975).
67. Goetz, C. G. et al. Movement Disorder Society-sponsored revision of the Unified Parkinson's Disease Rating Scale (MDS-UPDRS): scale presentation and clinimetric testing results. *Mov. Disord.* **23**, 2129–2170 (2008).
68. Cummings, J. et al. The Neuropsychiatric Inventory: comprehensive assessment of psychopathology in dementia. *Neurology* **44**, 2308–2314 (1994).
69. Beck, A. T., Steer, R. A., Ball, R. & Ranieri, W. F. Comparison of Beck depression inventories-IA and -II in psychiatric outpatients. *J. Pers. Assess.* **67**, 588–597 (1996).
70. Starkstein, S. E. et al. Reliability, validity, and clinical correlates of apathy in Parkinson's disease. *J. Neuropsychiatry Clin. Neurosci.* **4**, 149–151 (1992).
71. Chaudhuri, K. R. et al. International multicenter pilot study of the first comprehensive self-completed nonmotor symptoms questionnaire for Parkinson's disease: the NMSQuest study. *Mov. Disord.* **21**, 916–923 (2006).
72. Segura, B. et al. Cortical thinning associated with mild cognitive impairment in Parkinson's disease. *Mov. Disord.* **29**, 1495–1503 (2014).
73. Radhakrishnan, H., Bennett, I. J. & Stark, C. E. L. Higher-order multi-shell diffusion measures complement tensor metrics and volume in gray matter when predicting age and cognition. *Neuroimage* **253**, 119063 (2022).
74. Andersson, J. L. R., Skare, S. & Ashburner, J. How to correct susceptibility distortions in spin-echo echo-planar images: application to diffusion tensor imaging. *Neuroimage* **20**, 870–888 (2003).
75. Smith, S. M. Fast robust automated brain extraction. *Hum. Brain Mapp.* **17**, 143–155 (2002).
76. Andersson, J. L. R. & Sotiropoulos, S. N. An integrated approach to correction for off-resonance effects and subject movement in diffusion MR imaging. *Neuroimage* **125**, 1063–1078 (2016).
77. Graham, M. S., Drobnjak, I., Jenkinson, M. & Zhang, H. Quantitative assessment of the susceptibility artefact and its interaction with motion in diffusion MRI. *PLoS ONE* **12**, e0185647 (2017).

Acknowledgements

This study was sponsored by the Spanish Ministry of Economy and Competitiveness (MINECO PID2020-114640GB-I00 and PID2023-146932NB-I00 funded by MCI U/AEI/110.13039/5011000111033/FEDER, UE to C.J. and B.S.), Generalitat de Catalunya (SGR 2021SGR00801) and supported by María de Maeztu Unit of Excellence (Institute of Neurosciences, University of Barcelona) CEX2021-001159-M, the Spanish Ministry of Science and Innovation. This work was also supported by Fondo de Investigaciones Sanitario, Carlos III Health Institute (PI20/01473 to J.F.), the CIBERNED Program 1, the National Institutes of Health (NIH) grants (1R01AG056850-01A1; 3RF1AG056850-01S1; AG056850, R21AG056974, and R01AG061566 to J.F.), Departament de Salut de la Generalitat de Catalunya, Fundación Tatiana Pérez de Guzmán el Bueno (IIBSP-DOW-2020-151 to J.F.), and the European Union's Horizon 2020, 'MES-CoBraD' (H2020-SC1-BHC-2018-2020/GA 965422 to J.F.). J.P. was supported by a fellowship from the Ministry of Science and Innovation (PRE2021-099674). I.R. was supported by a fellowship from La Caixa Foundation (LCF/BQ/DR22/11950012). V.M. was supported by Predoctoral grants from the Carlos III Health Institute (FI18/00275). C.M.B. was supported by the María de Maeztu Unit of Excellence CEX2021-001159-M/financed by MICIU/AEI/10.13039/501100011033. J.O. was supported by a fellowship from the Ministry of Science, Innovation, and Universities (PRE2018-086675). The authors thank the patients, their relatives, and control subjects for their support in this study. We are also indebted to the Magnetic Resonance Imaging core facility of the FRCB-IDIBAPS for technical support, and we acknowledge the CERCA Programme/Generalitat de Catalunya.

Author contributions

B.S. and C.J. contributed to the design of the study. A.C., J.O., I.R. and J.P. contributed to the collection of the data. J.P., I.R. and C.M.B. contributed to the analyses of the data. J.P., V.M., A.C., J.O., I.R., C.M.B., J.F., C.J. and B.S. contributed to the interpretation of the data. J.P., I.R. and B.S. contributed to the writing of the first draft, and C.J. contributed to the final draft of the article. J.P., V.M., A.C., J.O., I.R., C.M.B., N.B., M.S., G.M., A.M., C.G., C.P.S., J.F., A.I., C.J. and B.S. revised the manuscript critically for important intellectual content and approved the final version of the manuscript.

Competing interests

J.F. reported receiving personal fees for service on the advisory boards, adjudication committees, or speaker honoraria from AC Immune, Alzheon, Novartis, Lundbeck, Roche, Fujirebio, and Biogen, outside the submitted work. J.F. reports holding a patent for markers of synaptopathy in neurodegenerative disease (licensed to ADx, EPI8382175.0). All other authors declare no competing interests.

Additional information

Supplementary information The online version contains supplementary material available at https://doi.org/10.1038/s41531-025-01058-0.

Correspondence and requests for materials should be addressed to Alex Iranzo or Bàrbara Segura.